PHYSICS AND CHEMISTRY OF SOLID STATE
V. 26, No. 3 (2025) pp. 598-606
Section: Physics

DOI: 10.15330/pcss.26.3.598-606

Vasyl Stefanyk Ccarpathian National University

ФІЗИКА І ХІМІЯ ТВЕРДОГО ТІЛА
Т. 26, № 3 (2025) С. 598-606
Фізико-математичні науки

PACS: 81.15.-z; 68.55.Ln

ISSN 1729-4428 (Print)
ISSN 2309-8589 (Online)

Abdelmalek Kharroubi[1], Hadj Benhebal[2], Bedhiaf Benrabah[1], Khaoula Hireche[1], Mohamed Touati[1], Yamina Loukrif[1]

Effect of tin doping on thin $SrCo_2O_4$ layers properties prepared by Sol-gel Dip-coating technique

[1]*Laboratory of Physical Engineering, Faculty of Mater Sciences, University of Tiaret, Algeria,*
[2]*Department of Chemstry, Faculty of Mater Sciences, University of Tiaret, Algeria, benhebalh@yahoo.fr*

Tin doped $SrCo_2O_4$ thin films at 0%, 3% and 5% on "pyrex" glass substrates have been prepared by Sol-gel Dip-coating method. In both cases cobalt nitrate, strontium nitrate and tin chloride were used as cobalt and strontium precursor and tin dopant source, respectively. X-ray diffraction analysis confirms the $SrCo_2O_4$ spinel crystal structure (311) as the preferential orientation with crystallite sizes ranging from 23.58 to 25.44 nm. Analysis of optical transmission spectra as a function of wavelength shows that transmission of the doped films is found to be superior to the undoped film and the band gaps (Eg) decreased from 1.48 to 1.43 eV by Sn dopants. Complex impedance spectroscopy indicates that the grain boundary effect is dominant in the mechanism of conduction. The resistance at the room temperature varied from 47.75 Ω to 41.87 Ω for variation of Sn concentration. The ICS results showed that the doped samples exhibit a smaller arc radius than the undoped sample, indicating faster electron transfer corresponding to lower electron transfer resistance at the surface.

Keywords: Sol-gel, $SrCo_2O_4$, Tin-doping, Dip-coating.

Received 07 October 2024; Accepted 17 August 2025.

Introduction

Modern scientific research has focused on the technology of production and processing of new materials in the form of nanostructured thin films because it allows the development of devices with excellent optoelectronic properties suitable for new technological applications [1]. Mixed oxides with spinel structure and general formula AB_2O_4 belong to the space group Fd-3m, where 32 oxygen ions form a cubic close-packed structure forming tetrahedral and octahedral sites (A and B sites, respectively) [2]. They are characterized by higher electrochemical activity and electrical conductivity than simple oxides, which makes them more widely used in many fields, especially for the production and storage of electrochemical energy [3-5]. Thus, ternary metal cobaltites (TMCs) constitute a special class of materials due to their multiple oxidation states, high charge storage capacity, enhanced electrical conductivity and thermodynamic stability [6]. Because of the low electrical conductivity of cobalt spinel oxide (Co_3O_4), several research studies propose reducing the Co content by substituting Co^{2+} in the tetrahedral sites of spinel structure with alkali metals, alkaline earth metals, metals from rare earths or certain other transition metals thus forming spinels with formulas MCo_2O_4 such as; $LiCo_2O_4$ [7], $MgCo_2O_4$ [8], $CaCo_2O_4$ [9], $NiCo_2O_4$ [10], $MnCo_2O_4$ [11], $CuCo_2O_4$ [12] and $ZnCo_2O_4$ [13]. In addition, it has been proven that the thermodynamic stability as well as the optoelectric characteristics of thin films strongly depends on the synthesis method and the optimization of the deposition conditions [14]. Many techniques have been suggested to obtain nanostructured thin films such as; vacuum evaporation, laser ablation, molecular beam epitaxy, sputtering, chemical vapor deposition, atomic layer epitaxy, spray pyrolysis and sol-gel in combination with spin coating or dip coating [15]. Sol-gel method in combination with dip-coating technique has become a simple and convenient technology for the low-temperature preparation of nanomaterials in various types such as;

nanopowders, fibers, nanotubes and thin films [16]. In this paper, nanostructured undoped and tin-doped strontium cobalt spinel oxide thin films were prepared by sol- gel dip-coating process. Physical properties, such as structural, optical and electrical were investigated using X-ray Diffraction (XRD), Fourier Transform Infrared (FTIR), UV-Visible spectroscopy and impedance complex spectroscopy (IC).

I. Experimental

1.1. Preparation of films

The synthesis was carried out by preparing three solutions in parallel. The first solution was obtained by dissolving 2.91 g of cobalt nitrate powder ($Co(NO_3)_2.6H_2O$) (Sigma Aldrich, 99.8%) in a volume of 120 ml of ethanol (C_2H_6O) (Sigma Aldrich, 99.8%). Magnetic stirring for 30 min resulted in the formation of a colored solution. The second is a solution of copper nitrates obtained by dissolving 4.36 g of strontium nitrate ($Sr(NO_3)_2$) in 120 ml of distilled water. After mixing the two solutions, the citric acid solution was added. The mixture was slowly heated to 80°C for 5 hours under magnetic stirring; this solution is characterized by a purple-red colour. Tin solutions were prepared using 2.91 g of a tin (II) chloride powder dissolved in ethanol and stirred for 2 hours. The solution obtained is transparent, yellow in colour and slightly viscous. Appropriate volumes of doping solutions were taken and added to the corresponding volumes taken from the mixture in order to obtain a doping rate (3% and 5%). The mixtures thus obtained were stirred and then spread by immersion on pyrex glass substrates well cleaned. After removing the glasses, the layers obtained were dried at 100° before being heat treated at 500°C. This protocol is well detailed in Figure (1).

1.2. Characterization

The structural characterization was analyzed using a Philips PW1830 X-ray diffractometer with (CuKα) radiation with copper anticathode (I = 30 mA; V = 40 KV and λ = 1.5406 Å). The optical transmittance of the films

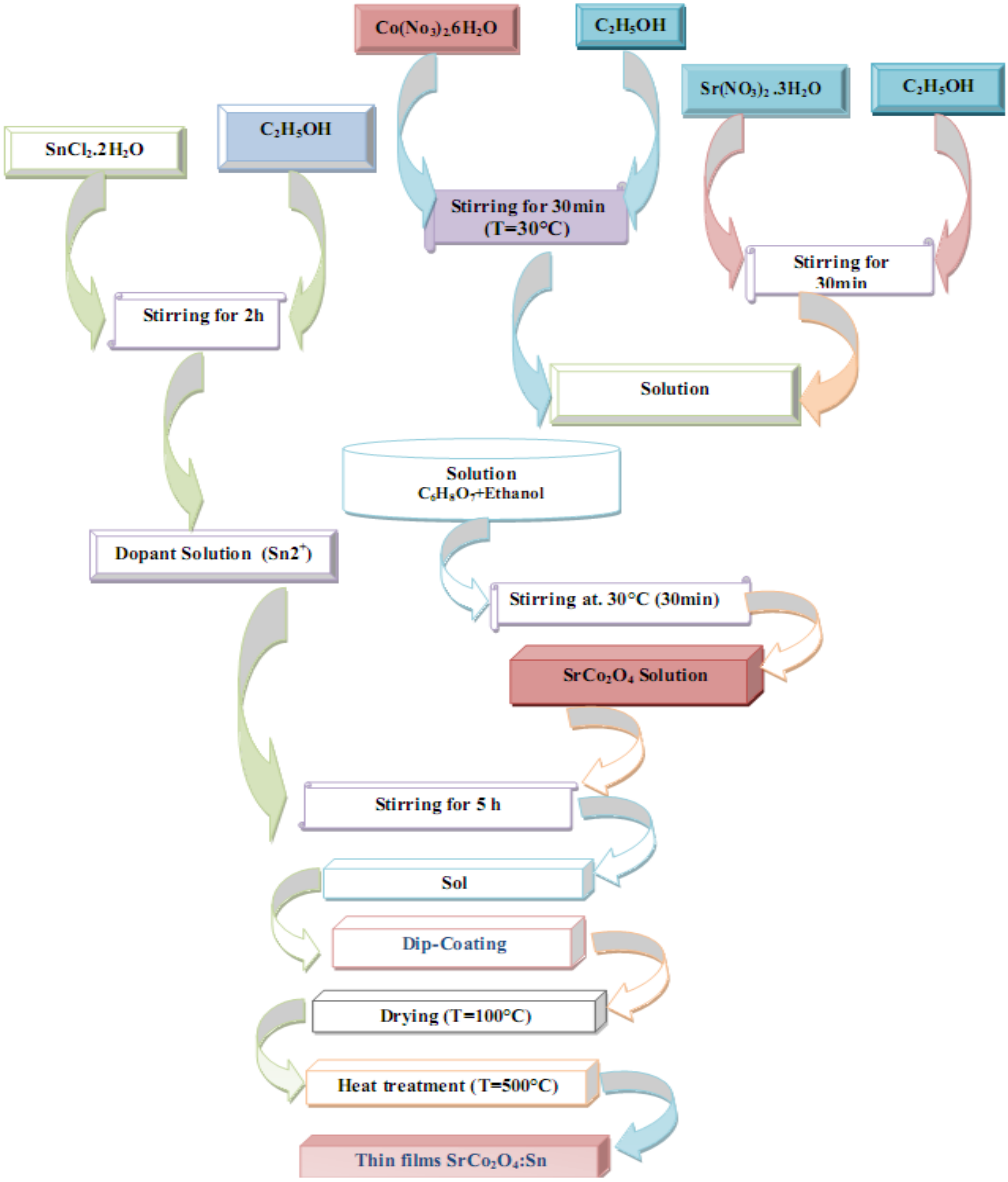

Fig. 1. Schematic diagram of the experimental protocol for the preparation of undoped and tin-doped $SrCo_2O_4$ thin films.

was measured using UV-1650 Shimadzu spectrophotometer in the wavelength range from 300 to 900 nm. FTIR spectra of the samples were recorded using a Shimadzu 8400 Spectrometer in the wave number range from 400 cm^{-1} to 4000 cm^{-1}. Impedance measurements were performed using the Agilent4284A LCR meter operating in the frequency range of 75 kHz to 20 MHz with oscillation amplitude of 1 V.

II. Results and discussion

2.1. Structural analysis (DRX)

Figure.2. shows the diffractograms of undoped and Sn-doped $SrCo_2O_4$. The diffractograms thus obtained present reflections similar to those of Co_3O_4 corresponding to the face centre cubic phase which matched with JCPDS No. 00-042-1467 with FD-3m space group with a preferred (311) orientation [17]. There were small peaks from impurity phases such as $CoCO_3$ (standard JCPDS file n°.78-0209) [18,19]. No peaks associated with the SnO_2 phase were detected with increasing Sn concentrations, indicating that tin ions are uniformly incorporated into the $SrCo_2O_4$ lattice. It can be observed that the cubic planes of the spinel phase exhibit a slight shift with increasing Sn content. The apparent diffraction peaks indicated the formation of well-crystallized $SrCo_2O_4$ nanoparticles. It should be noted that the crystallinity is much more developed for the sample with 3% doping.

The most intense reflection corresponding to the (311) plane was used to calculate the average crystallite size (D) of $SrCo_2O_4$ nanoparticles [20], using Scherrer equation (1):

$$D = K\lambda/\beta cos\theta \quad (1)$$

Where K= 0.9, λ is the X-ray wavelength, β is the full width at half maximum of the XRD peak, θ is the Bragg diffraction angle.

The microstrain (ε) and the in the deposited films is calculated from the slope of βcosθ vs. 2sinθ plot using the formula given below (2) [21,22]:

$$\varepsilon = \beta cos\theta/4 \quad (2)$$

On the other hand, the dislocation density (δ) is calculated using the formula given below [21,22]:

$$\delta = 1/D^2 \quad (3)$$

The calculated values of average crystallite size (D), average microstrain (ε) and dislocation density (δ) presented in Table 1 were plotted as a function of Sn content as shown in Fig 3.

The values of the average crystallite sizes (D) of the undoped, 3% Sn- and 5% Sn-doped $SrCo_2O_4$ thin films (table 1), are 23.58 nm, 24.03 nm and 25.44 nm, respectively. The obtained microstrain values are positive and increase following the doping of tin in the $SrCo_2O_4$ spinel indicating the tensile stress [23]. As shown in the figure 3, the increase in dislocation density and micro-strain shows that the $SrCo_2O_4$ lattice is destabilized by tin doping [24]. This decrease in the dislocation density can be justified by a weak inperfection of the lattice caused by the reduction in the occurrence of grain boundaries and the increase crystallites size [25].

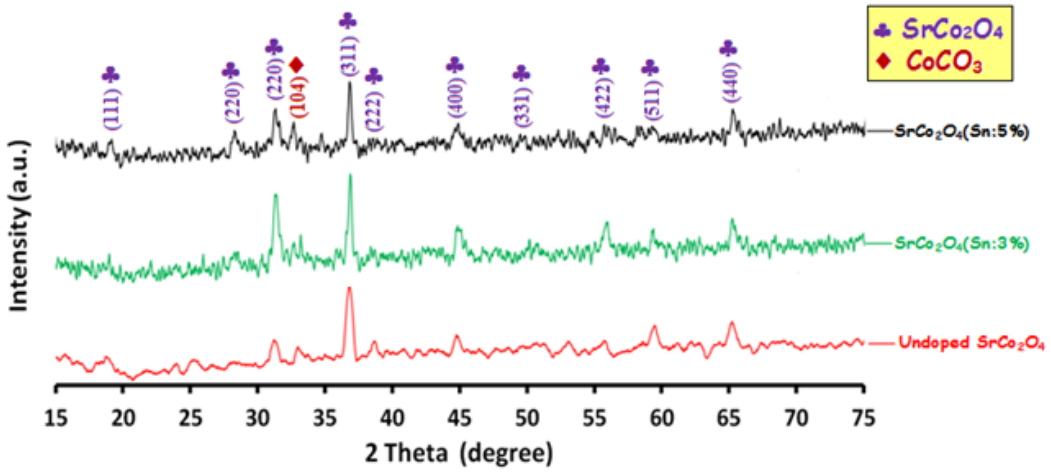

Fig. 2. The X-ray diffraction patterns of Sn:$SrCo_2O_4$ thin layers.

Table 1.

FWHM, crystalline size, strain and dislocation density of pure and Sndoped $SrCo_2O_4$ thin films

Sample	FWHM (β) (rad)	Cristallite size (nm)	Microstrain (10^{-3})	Dislocation density (10^{-3}) nm^{-2}
Undoped $SrCo_2O_4$	0,0125	23.58	1.39	1.79
$SrCo_2O_4$:Sn(3%)	0,00676	24.03	1.60	1.73
$SrCo_2O_4$:Sn(5%)	0,00638	25.44	1.53	1.54

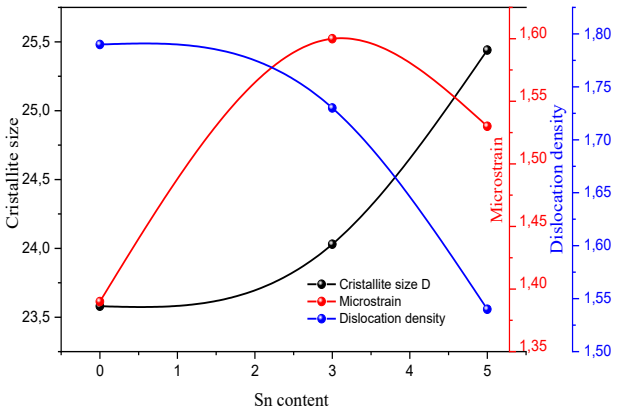

Fig. 3. Variation of crystallite size, microstrain and dislocation density of pure and Sn-doped $SrCo_2O_4$ thin films.

2.2. Optical analysis

Fig. 4 shows the transmittance spectra of pure and Sn-doped $SrCo_2O_4$ thin films with different tin concentration. It observed that all the as prepared films were highly transparent in the visible range. The transmittance shows an increasing tendency with increasing tin doping. The average value of transmittance increases from 82% to 95% as tin concentration increases from 0% to 5%. The observed results are in good agreement with similar investigations on the Sn-doped nanostructured thin films [26,27].

As reported in numerous studies in the literature [28-31], the absorbance spectrum of cobalt-based spinel oxides MCo_2O_4 contains two distinct regions with absorption maxima. The first region is attributed to the transition from the valence band to the conduction band, which is the fundamental absorption transition ($O^{2-} \rightarrow M^{2+}$), while the other is attributed to the transition from the valence band to the band that is created as a sub-band by Co^{3+} ions and located below the conduction band. Consequently, a double band gap structure with two optical band gaps, Eg_1 and Eg_2 [32].

Assuming that the cobaltite spinel structure is known to be a direct band gap material [33], the optical band gap of pure and Sn-doped $SrCo_2O_4$ thin films are computed from Tauc's plot [34,35] between hν (eV) and $(\alpha h\nu)^2$, using the following equation:

$$(ahv) = A^*(hv - Eg)^{1/2} \qquad (4)$$

Here, α is the absorption coefficient, hν is the photon energy, A is a constant, Eg is the optical bandgap energy and the value of the exponent (n =1/2) in the right-hand side means that the authorized transition is indirect.

As shown in Figure 5, two linear regions appear, indicating the existence of two different band gap energy values. The computed band gap values as indicated in Table 2 and presented in figure 5, decreases for direct transitions when the Sn-content increases in the 3% and 5% Sn/$SrCo_2O_4$.

2.3. FT-IR spectroscopy

FTIR spectra (Figure 6) demonstrated two strong absorption bands at 670 and 580 cm^{-1}, which confirms the formation of the spinel structure of cobaltite [36,37]. The first peak is attributed to the stretching vibrational mode of M–O in which M is Co^{2+} or Sr^{2+} tetrahedrally coordinated [38]. The second peak can be attributed to M–O in which M is Co^{3+} octahedrally coordinated [39]. The observed symmetric metal-oxygen stretching vibrations at the tetrahedral and octahedral sites confirm the formation of the spinel structure [40]. The two peaks located at 1458 cm^{-1} and 875 cm^{-1} are assigned to the ν_3 vibration mode and ν_2 vibration mode of free, planar carbonates (CO_3^{2-}) ions (group symmetry D_3H) [41]. The band observed at approximately 3400 cm^{-1} is due to O–H stretching assigned to adsorbed water on the metal surface [42]. The FTIR bands of the spinel structure shift slightly to lower wavenumbers after tin doping. This shift can be explained by the slowing down of the vibration of chemical bonds due to the increase in molecular weight [43].

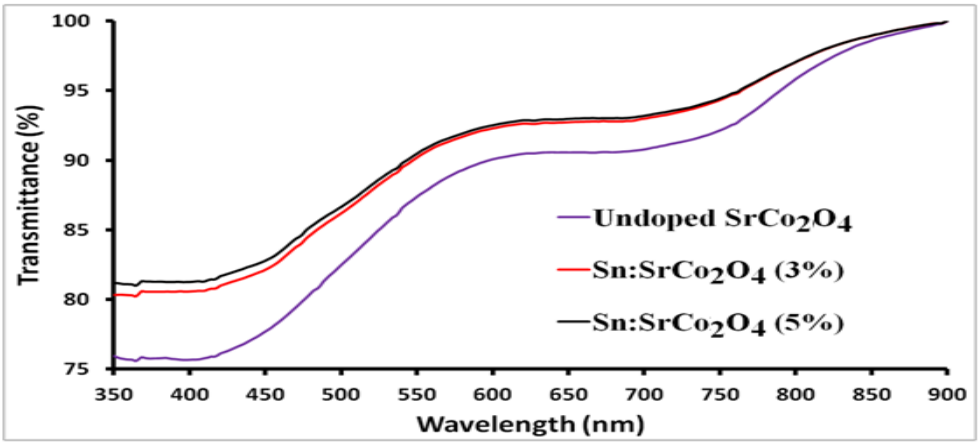

Fig. 4. Transmittance spectra of pure and Sn-doped $SrCo_2O_4$ thin Films.

Table 2.

Estimated optical band gap energy values of undoped and Sn-doped $SrCo_2O_4$ thin films.

Samples	Undoped $SrCo_2O_4$	$SrCo_2O_4$:Sn3%	$SrCo_2O_4$:Sn5%
Eg_1 (eV)	1.48	1.45	1.43
Eg_2 (eV)	1.76	1.74	1.71

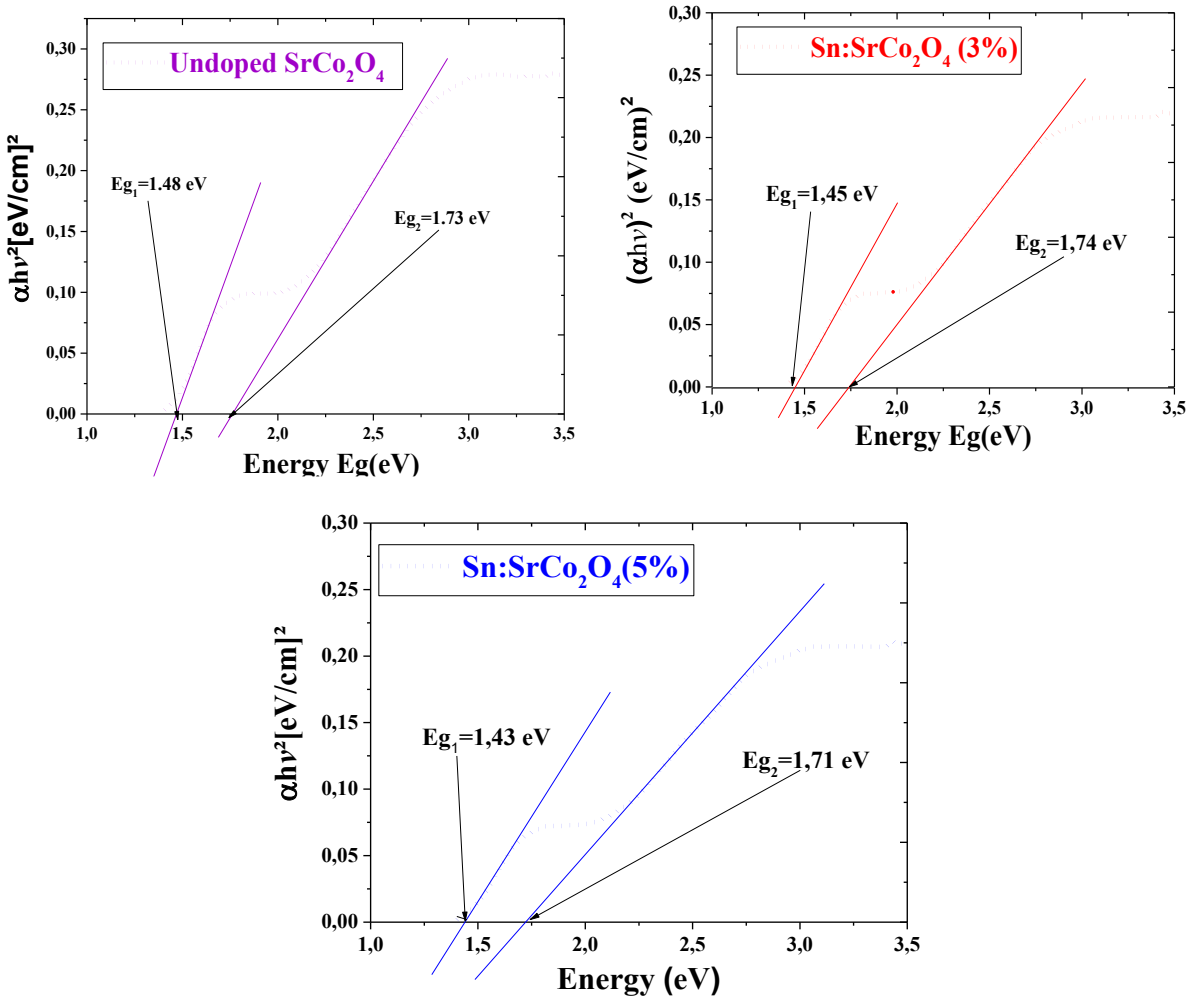

Fig .5. Tauc plots of pure and Sn-doped $SrCo_2O_4$ thin Films.

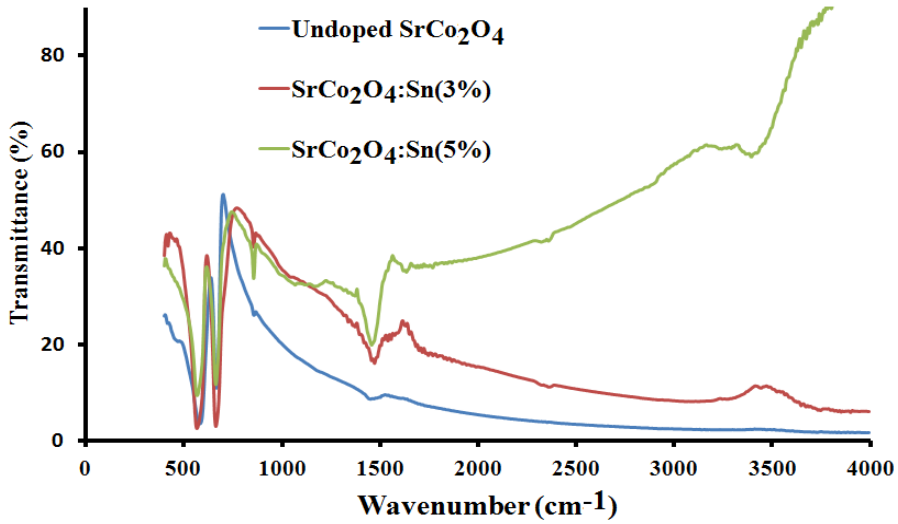

Fig.6. FT-IR spectra of undoped and Sn-doped $SrCo_2O_4$ thin Films.

2.4. Impedance spectroscopy

Using complex impedance spectroscopy (CIS), the electrical properties of pure and tin-doped strontium cobaltite thin films were studied. Figure 7 depicts the Nyquist plots (Z" vs. Z') of pure and doped $SrCo_2O_4$ thin films, measured from the complex impedance under standard illumination conditions, in the range of 75 kHz to 20 MHz and at an applied potential of 1V. The Nyquist diagram for undoped and Sn-doped $SrCo_2O_4$ films (figure 7) shows semicircles. The impedance parameters were estimated by considering the equivalent circuit of the samples shown in the inset of the figure, consisting of a parallel RC circuit. It was noticed that the value of Z' and Z'' in the spectra decreases with increasing doping concentration, suggesting that the net resistance of $SrCo_2O_4$ nanoparticles decreases steadily [44].

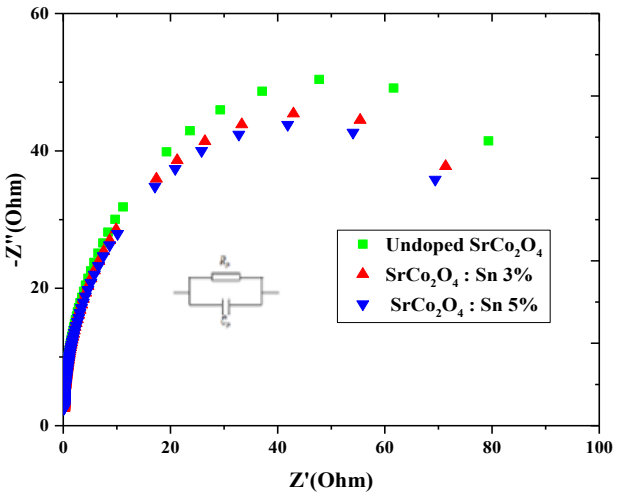

Fig.7. Nyquist plots of pure and Sn-doped $SrCo_2O_4$ thin Films.

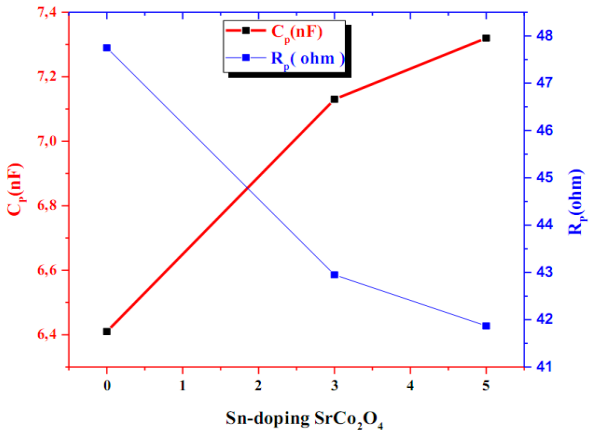

Fig.8. Variation of Rp and Cp as a function of tin doping.

As shown in the fitted results (Table 3) and plotted (Figure 8), the resistance Rp decreased from 47.75 to 41.87 ohms, while the capacitance increased from 6.41 to 7.32 nF. The thin films of the tin-doped samples exhibit reduced resistance compared to the doped sample due to the incorporation of Sn^{4+} and the consequent improvement in conductivity [45]. Sn-doped thin films showed reduced electron transport resistance and high capacitance compared to undoped $SrCo_2O_4$, which is consistent with the enhanced electrical conductivity over Sn^{4+} [46]. Indeed, doped nanoparticles develop a larger surface area. This structure is characterized by greater electronic recombination induced by the electron hopping mechanism and consequently lower resistance to electronic transport, which is consistent with several results reported in the literature [47,48].

Table 3.
Values of: fmax, Rp, and Cp of undoped and Sn-doped $SrCo_2O_4$ thin Films.

Samples	F_{max}(KHZ)	R(Ω)	C (nF)
Undoped $SrCo_2O_4$	519.44	47.75	6.41
$SrCo_2O_4$:Sn(3%)	519.44	42.95	7.13
$SrCo_2O_4$:Sn (5%)	519.44	41.87	7.32

Conclusion:

Sn-doped $SrCo_2O_4$ thin films were prepared by sol-gel dip-coating method on a pyrex glass substrate. The effect of Sn doping on the structural, optical and electrical properties of $SrCo_2O_4$ thin films was studied. The deposited films of pure and Sn-doped $SrCo_2O_4$ showed good crystallinity of cubic spinel structure and retain their preferential orientation (311). The crystallite size of the samples increased as increasing Sn doping concentrations. Optical spectra show that all films exhibit good transparency of about 85% in the visible region. The optical band gap of the films is decreasing with increasing Sn content. The complex impedance spectroscopy indicates that the effect of the grain joints is dominant in the conduction mechanism; we also note that the equivalent pattern of $SrCo_2O_4$ films for each incorporation rates is a parallel RC circuit.

Acknowledgement:
We would like to thanks Prof. El-Habib BELARBI head of the Synthesis and Catalysis Laboratory of the Faculty of Meter Sciences at the University of Tiaret for all the measurements carried out within the framework of this work.

Abdelmalek Kharroubi – HDR.(physics), Teacher researcher.Aboulkacem Khiali –Doctor of Engineering Sciences;
Hadj Benhebal – Professor, Professorat the Department of Chemistry;
Bedhiaf Benrabah – Professor, Professorat the departmentofphysics;
Khaoula Hireche – PhD. Ph.D. Student (Physics);
Mohamed Touati – Ph.D. Student (Physics);
Yamina Loukrif – Master Student (physics).

[1] H. Buzhabadi, M B. Rahmani and M. Damghani., *Investigation of Sn-doped WO_3 thin films: One-step deposition by hydrothermal technique, characterization, and photoluminescence study*. Modern. Phys. Lett. B, 38(30), 2450163 (2024); https://doi.org/10.1142/S021798492450163X.
[2] N. Danyliuk, I. Lapchuk, V. Kotsyubynsky, V. Boychuk, V. Husak., *Effect of Mn^{2+}substitution on catalytic properties of $Fe_{3-x}Mn_xO_4$ nanoparticles synthesized via co-precipitation method*. Phys. Chem. Solid State, 24, 748 (2023); https://doi.org/10.15330/ pcss.24.4.748-76.
[3] J M. Gonçalves, M I. da Silva, M N. T. Silva, P R. Martins, E. Nossol, H E. Toma and L. Angnes., *Recent progress in $ZnCo_2O_4$ and its composites for energy storage and conversion: a review.* Energy Adv., 1, 793 (2022); https://doi.org/10.1039/D2YA00106C.

[4] Sathyanarayana Neelam, Rakeshkumar Thida,Shilpa Chakra Chidurala, Srinivasu Daripaalli, Ravinder Reddy Butreddy, *Enhanced Structural and Electrochemical properties of spinel structured Ca doped nickel cobaltite nanoparticles synthesized by microwave hydrothermal method*. Int. J. Eng. Res. Appl., 13, 5, 29 (2023); https://doi.org/10.9790/9622-1305294129.

[5] T.H. Dolla, I.A. Lawal, G.W. Kifle, et al. *Mesoporous Mn-substituted $Mn_xZn_{1-x}Co_2O_4$ ternary spinel microspheres with enhanced electrochemical performance for supercapacitor applications*. Scientifc Reports, 14, 11420 (2024); https://doi.org/10.1038/s41598-024-58822-0.

[6] S G. Krishnan, A. Arulraj, M. Khalid, M.V. Reddy and R. Jose., *Energy storage in metal cobaltite electrodes: Opportunities & challenges in magnesium cobalt oxide. Renew*. Sustain. Energy Rev., 141, 110798 (2021); https://doi.org/10.1016/j.rser.2021.110798.

[7] Y. Mouhib, M. Belaiche, C. A Ferdi, M Lacham and A Elacham., *New Technique for Elaboration and Characterization of High Voltage Spinel $LiCo_2O_4$ Cathode and Theoretical Investigation*. New J. Chem. 44, 2538 (2020); https://doi.org/10.1039/C9NJ06126F.

[8] M. Mahinzad Ghaziani, J. Mazloom, F.E. Ghodsi., *Electrospun $MgCo_2O_4$ nanofibers as an efficient electrode material for pseudocapacitor applications: Effect of calcination temperature on electrochemical performance*. Journal of Physics and Chemistry of Solids, 152 109981 (2021); https://doi.org/10.1016/j.jpcs.2021.109981.

[9] M. Cabello, F. Nacimiento, JR. Gonz´alez, G. Ortiz, R. Alcantara, P. Lavela, C. Pérez-Vicente and J L. Tirado, *Advancing towards a veritable calcium-ion battery: $CaCo_2O_4$ positive electrode material*. Electrochem Commun., 67, 59 (2016); https://doi.org/10.1016/j.elecom.2016.03.016.

[10] Hengli Qian, keyuan Zhang, Yongchuo He, Qidong Hou, Chao Xie, Ruite Lai, Guanjie Yu, Tianliang Xia, Xinyu Bai, Haijiao Xie, Meiting Ju., *Engineering crystal plane of $NiCo_2O_4$ to regulate oxygen vacancies and acid sites for alkali-free oxidation of 5-hydroxymethylfurfural to 2,5-furandicarboxylic acid*. Green Energy & Environment, 10(4), 756 (2025); https://doi.org/10.1016/j.gee.2024.05.002.

[11] Maha Alhaddad, Reda M. Mohamed, Mohamed H. H. Mahmoud., *Promoting Visible Light Generation of Hydrogen Using a Sol–Gel-Prepared $MnCo_2O_4$@g-C_3N_4 p–n Heterojunction Photocatalyst*. : ACS Omega, 6, 8717 (2021); https://doi.org/10.1021/acsomega.1c00697.

[12] MV. Reddy, M. Rajesh, S. Adams, BVR. Chowdari, *Effect of initial reactants and reaction temperature on molten salt synthesis of $CuCo_2O_4$ and its sustainable*. ACS Sustainable. Chem. Eng., 4(6), 3076 (2016); https://doi.org/10.1021/acssuschemeng.6b00047.

[13] Awaltanova, E., Amri, A., Mondinos, N. et al. *Nanorose-like $ZnCo_2O_4$ coatings synthesized via sol–gel route: morphology, grain growth and DFT simulations*. J Sol-Gel Sci Technol, 90, 450 (2019); https://doi.org/10.1007/s10971-019-04987-4.

[14] Subramanian Sakthinathan, Ganesh Abinaya Meenakshi, Sivaramakrishnan Vinothini, Chung-Lun Yu, Ching-Lung Chen, Te-Wei Chiu and Naratip Vittayakorn., *A Review of Thin-Film Growth, Properties*, Applications, and Future Prospects. Processes, 13, 587 (2025); https://doi.org/10.3390/pr13020587.

[15] M. Dramićanin, *Lanthanide and Transition Metal Ion Doped Materials for Luminescence Temperature Sensing, Chapter 6. Luminescence Thermometry Methods, Materials, and Applications*. Woodhead Publishing Series in Electronic and Optical Materials. 113 (2018); https://doi.org/10.1016/B978-0-08-102029-6.00006-3.

[16] G. Balakrishnan, P K. Ray, R. Kumar, R K. Chaudhary, R. Kumar, P K. Roy and R. Gopinath, *Preparation of alumina (Al_2O_3) thin films by sol-gel dip coating and characterization*. Int. J Current. Adv. Res., 6, 6099 (2017); http://dx.doi.org/10.24327/ijcar.2017.6103.0873.

[17] E.U. Ikhuoria, et al., *Bioinspired shape controlled antiferromagnetic Co_3O_4 with prism likeanchored octahedron morphology: A facile green synthesis using Manihot esculenta Crantz extract*, Sci. Technol. Mater., (2018); https://doi.org/10.1016/j.stmat.2018.02.003.

[18] S. Yuvaraj, A. Vignesh, S. Shanmugam, R. Kalai Selvan, *Nitrogen-doped Multi-walled Carbon Nanotubes $MnCo_2O_4$ microsphere as electrocatalyst for efficient oxygen reduction reaction*. Int. J. Hydrogen Energy, 41, 15199 (2016); http://dx.doi.org/10.1016/ j.ijhydene.2016.06.115.

[19] M. H. Oza, D. K. Kanchan, J. H. Joshi, M. J. Joshi, Structural, *DFT, vibrational spectroscopic, thermal, electricaland magnetic characterizations of hydrothermally grown $CoCO_3$ microcrystals*. J. Mater. Sci.: Mater. Electron., 31,10177 (2020); https://doi.org/10.1007/s10854-020-03563-9.

[20] R. Zapukhlyak, M. Hodlevsky, V. Boychuk, J. Mazurenko, V. Kotsyubynsky, L. Turovska, B. Rachiy, S. Fedorchenko, *Structure and magnetic properties of hydrothermally synthesized $CuFe_2O_4$ and $CuFe_2O_4$/rGO composites*. J. Magn. Magn. Mater., 587, 171208 (2023); https://doi.org/10.1016/j.jmmm.2023.171208.

[21] G.B. Williamson and R.C. Smallman, *Dislocation densities in some annealed and cold-worked metals from measurements on the X-ray debye-scherrer spectrum*, Phil. Mag., 1(1), 34 (1956); https://doi.org/10.1080/14786435608238074.

[22] L. Kaykan, A.K. Sijo, A. Żywczak, K. Bandura. *Tailoring of structural and magnetic properties of nanosized lithium ferrites synthesized by sol–gel self-combustion method*. Appl Nanosci., 10, 4577 (2020); https://doi.org/10.1007/s13204-020-01413-y.

[23] S. Kuriakose, V. Choudhary, B. Satpatib, S. Mohapatra, *Enhanced photocatalytic activity of Co doped ZnO nanodisks and nanorods prepared by a facile wet chemical method*, Phys. Chem. Chem. Phys., 17, 12741 (2014); https://doi.org/10.1039/c4cp01315h.

[24] A. El-Habib, M. Addou, A. Aouni, M. Diani, J. Zimou andH. Bakkali., *Synthesis, structural and optical characteristics of vanadium doped cerium dioxide layers*. Materialia, 18, 101143 (2021); https://doi.org/10.1016/j.mtla.2021.101143.

[25] A. Begum, A. Hussain and A. Rahman, *Effect of deposition temperature on the structural and optical properties of chemically prepared nanocrystalline lead selenide thin films*. Beilstein J. Nanotechnol., 3, 438 (2012); https://doi.org/10.3762/bjnano.3.50.

[26] Z. Zhao, Y. Liu, D. Wang, C. Ling, Q. Chang, J. Li, Y. Zhao and H. Jin, *Sn dopants improve the visible transmittance of VO_2 films achieving excellent thermochromic performance for smart window*. Sol. Energy Mater. Sol. Cells, 209, 110443 (2020); https://doi.org/10.1016/j.solmat.2020.110443.

[27] S. Aziz, Md. A. A. Shaikh, M. Hossain and M. S. Shah Jamal, *Influence of Sn doping on the optoelectronic properties of ZnO nanoparticles*. Nanoscale Adv., 5, 4996 (2023); https://doi.org/10.1039/D3NA00409K.

[28] P. Prieto, J.F. Marco, A. Serrano, M. Manso, J. de la Figuera, *Highly oriented (111) CoO and Co_3O_4 thin films grown by ion beam sputtering.* J. Alloys Compd., 810, 151912 (2019); https://doi.org/10.1016/j.jallcom.2019.151912].

[29] L. Abdelhak, B. Amar, B. Bedhiaf, D. Cherifa, B. Hadj, *Characterization of Mn-Doped Co_3O_4 thin films prepared by sol-gel-based dip-coating process.* High Temp. Mater. Process, 38, 237 (2019); https://doi.org/10.1515/htmp-2017-0185.

[30] N. Kouidri, S. Rahmane, A. Allag, *Substrate temperature-dependent properties of sprayed cobalt oxide thin films.* J. Mater. Sci. Mater. Electron., 30, 1153 (2019); https://doi.org/10.1007/s10854-018-0384-3.

[31] A. Kucukarslan, E. Kus, E. Sarica, I. Akyuz, V. Bilgin, B. Demirselcuk., *Improvement of structural, optical and magnetic properties of cobalt oxide thin films by doping with iron.* Appl. Phys. A, 127, 512 (2021); https://doi.org/10.1007/s00339-021-04672-w.

[32] A. Abdelmoneim, A. Naji, E. Wagenaars, M. Shaban, *Outstanding stability and photoelectrochemical catalytic performance of (Fe, Ni) co-doped Co_3O_4 photoelectrodes for solar hydrogen production*. Int. J. Hydrogen Energy, 46, 12915 (2021); https://doi.org /10.1016/j.ijhydene.2021.01.113.

[33] J. O. D. Malafatti, A. JoséMoreira, E. C. Paris, L. J. C. Flechas, O. A. P. Pereira, M. R. Joya, *Evaluation of Ni-Doped Tricobalt Tetroxide with Reduced Graphene Oxide: Structural, Photocatalysis, and Antibacterial Response*. catalysts Catalysts, 12, 1199 (2022); https://doi.org/10.3390/catal12101199.

[34] R. Bhatt, I. Bhaumik, S. Ganesamoorthy, A.K. Karnal, M.K. Swami, H.S. Patel and P.K. Gupta, *Urbach tail and bandgap analysis in near stoichiometric $LiNbO_3$ crystal*s. Phys. Status. Solidi, A, 209, 176 (2012); https://doi.org/10.1002/pssa.201127361.

[35] J. Mazurenko, A. K. Sijo, L. Kaykan, V. Kotsyubynsky, Ł. Gondek, A. Zywczak, M. Marzec, O. Vyshnevsky, *Synthesis and Characterization of Copper Ferrite Nanoparticles for Efficient Photocatalytic Degradation of Organic Dye*s. J. Nanotechnology, 2025, 26 pages (2025); https://doi.org/10.1155/jnt/8899491.

[36] M.Y. Nassar, I.S. Ahmed, *Hydrothermal synthesis of cobalt carbonates using different counter ions: An efficient precursor to nano sized cobalt oxide (Co_3O_4)*. Polyhedron. 30, 2431 (2011); https://doi.org/10.1016/j.poly.2011.05.039.

[37] B. Sreedhar, M. Sulochana, C.S. Vani, D.K. Devi, N.V.S. Naidu, *Shape evolution of strontium carbonate architectures using natural gums as crystal growth modifiers*, Eur. Chem. Bull., 3, 234 (2014); https://www.eurchembull.com.

[38] P. Ptáčekn, E. Bartoníčková, J. Švec, T. Opravil, F. Šoukal, F. Frajkorová, *The kinetics and mechanism of thermal decomposition of $SrCO_3$ polymorphs*, Ceram. Int, 41, 115 (2015); https://doi.org/10.1016/j.ceramint.2014.08.043.

[39] M. Sun, Y. Jiang, F.F. Li, M.S. Xia, B. Xue, D.R. Liu, *Effect of oxygen vacancy variation on the photo-assisted degradation and structural phase transition of oxygen defective $Ba(Fe,Co)O_{3-x}$,* Mater. Res. Bull, 46, 801 (2011); https://doi.org/10.1016/j.materresbull.2011.02.036.

[40] J. Mazurenko, L. Kaykan, K. Bandura, O. Vyshnevskyi, M. Moiseienko, M. Kuzyshyn, N. Ostapovych, *Analysis of the Structural, Morphological, and Elastic Properties of Nanosized CuFe2O4Spinel Synthesized via Sol-Gel Self-Combustion Method*. Phys. Chem. Solid State, 25, 380 (2024); https://doi.org/10.15330/pcss.25.2.380-390.

[41] G. Pandey, K N. Dhakal, A K. Singh, S K. Dhungel, R. Adhikari, *Facile methods of preparing pure hydroxyapatite nanoparticles in ordinary laboratories.* Bibechana 18, 83 (2021); https://doi.org/10.3126/bibechana.v18i1.29600.

[42] N. Ahammed, MD Samim Hassan and M. Hassan, *Effects of aluminum (Al) incorporation on structural, optical and thermal properties of ZnO nanoparticles.* Mater. Sci.-Pol., 36, 1 (2018). https://doi.org/10.1515/msp-2018-0018.

[43] K. Kayed, M. Issa, H. Al-ourabi, *The FTIR spectra of Ag/Ag_2O composites doped with silver nanoparticles*, J. Exp. Nanosci., 19, 2336227 (2024); https://doi.org/10.1080/ 17458080.2024.2336227.

[44] N. Khatun, S. Ahmed, M S. Hossain, S F U. Farhad, Md Al- Mamun, M. S. Alam, M. H A. Begum, N I. Tanvir, M. Hakim, S. Islam, *Influence of Y^{3+} and La^{3+} ions on the structural, magnetic, electrical, and optical properties of cobalt ferrite nanoparticles*. Heliyon, 9, e13019. (2023); https://doi.org/10.1016/j.heliyon.2023.e13019.

[45] A. Annamalai, H. Lee, S. Choi, et al. *Sn/Be Sequentially co-doped Hematite Photoanodes for Enhanced Photoelectrochemical Water Oxidation: Effect of Be^{2+} as co-dopant*. Scientific Reports, 6, 23183 (2016); https://doi.org/10.1038/srep23183.

[46] A. Annamalai, H H. Lee, S. H. Choi, SY. Lee, E. Gracia-Espino, A. Subramanian, J. Park, K J. Kong, J S. Jang, *Sn/Be Sequentially co-doped Hematite Photoanodes for Enhanced Photoelectrochemical Water Oxidation: Effect of Be^{2+} as co-dopant*. Scientific Reports, 6, 23183 (2016); https://doi.org/10.1038/srep23183.

[47] A. Annamalai, P S. Shinde, T H. Jeon, H H. Lee, H G. Kim, W. Choi, J S. Jang, *Fabrication of superior α-Fe_2O_3 nanorod photoanodes through ex-situ Sn-doping for solar water splitting. Sol*. Energy Mater. Sol. Cells, 144, 247 (2016); http://dx.doi.org/10.1016/ j.solmat.2015.09.016.

[48] A. Zulkiflee, M M. Khan, A. Khan, M Y. Khan, H D M. Dafalla, M H. Harunsani, *Sn-doped BiOCl for photoelectrochemical activities and photocatalytic dye degradation under visible light*. Heliyon, 9, e21270 (2023); https://doi.org/10.1016/j.heliyon.2023.e21270.

Абдельмалек Харрубі[1], Хадж Бенхебал[2], Бедхіаф Бенрабах[1], Кхаула Гірече[1], Мохамед Туаті[1], Яміна Лоукріф[1]

Вплив легування оловом на властивості тонких шарів $SrCo_2O_4$, отриманих методом золь-гель занурення

[1]*Лабораторія фізичної інженерії, факультет природничих наук, Університет Тіарет, Алжир;*
[2]*Кафедра хімії факультету природничих наук Університету Тіарет, Алжир, benhebalh@yahoo.fr*

Тонкі плівки $SrCo_2O_4$, леговані оловом, з вмістом 0%, 3% і 5% на підкладках зі скла "пірекс" були виготовлені методом золь-гель занурення. В обох випадках нітрат кобальту, нітрат стронцію та хлорид олова використовувалися як попередник кобальту та стронцію та джерело допанту олова відповідно. Рентгеноструктурний аналіз підтверджує кристалічну структуру шпінелі $SrCo_2O_4$ (311) як переважну орієнтацію з розмірами кристалітів від 23,58 до 25,44 нм. Аналіз спектрів оптичного пропускання як функції довжини хвилі показує, що пропускання легованих плівок виявляється кращим, ніж нелегованої плівки, а ширина забороненої зони (Eg) зменшилася з 1,48 до 1,43 еВ за допомогою легуючих домішок Sn. Спектроскопія комплексного імпедансу показує, що зернограничний ефект є домінуючим у механізмі провідності. Опір при кімнатній температурі змінювався від 47,75 Ом до 41,87 Ом для зміни концентрації Sn.

Ключові слова: золь-гель, $SrCo_2O_4$, легування оловом, занурення.